LANGMUIR Article
Cite This: Langmuir 2018, 34, 7153−7160
pubs.acs.org/Langmuir

Fate of Fluorescence Labels—Their Adsorption and Desorption Kinetics to Silver Nanoparticles

Claudia Kästner,[†] Linda Böhmert,[‡] Albert Braeuning,[‡] Alfonso Lampen,[‡] and Andreas F. Thünemann*[,†]

[†]Bundesanstalt für Materialforschung und -prüfung (BAM), Unter den Eichen 87, 12205 Berlin, Germany
[‡]Bundesinstitut für Risikobewertung (BfR), Max-Dohrn-Straße 8-10, 10589 Berlin, Germany

Supporting Information

ABSTRACT: Silver nanoparticles are among the most widely used and produced nanoparticles. Because of their frequent application in consumer products, the assessment of their toxicological potential has seen a renewed importance. A major difficulty is the traceability of nanoparticles in in vitro and in vivo experiments. Even if the particles are labeled, for example, by a fluorescent marker, the dynamic exchange of ligands often prohibits their spatial localization. Our study provides an insight into the adsorption and desorption kinetics of two different fluorescent labels on silver nanoparticles with a core radius of 3 nm by dynamic light scattering, small-angle X-ray scattering, and fluorescence spectroscopy. We used BSA-FITC and tyrosine as examples for common fluorescent ligands. It is shown that the adsorption of BSA-FITC takes at least 3 days, whereas tyrosine adsorbs immediately. The quantitative amount of stabilizer on the particle surface was determined by fluorescence spectroscopy and revealed that the particles are stabilized by a monolayer of BSA-FITC (corresponding to 20 ± 9 molecules), whereas tyrosine forms a multilayered structure consisting of 15900 ± 200 molecules. Desorption experiments show that the BSA-FITC-stabilized particles are ideally suited for application in in vitro and in vivo experiments because the ligand desorption takes several days. Depending on the BSA concentration in the particles surroundings, the rate constant is k = 0.2 per day or lower when applying first order kinetics, that is, 50% of the BSA-FITC molecules are released from the particle's surface within 3.4 days. For illustration, we provide a first application of the fluorescence-labeled particles in an uptake study with two different commonly used cell lines, the human liver cell model HepG2 and the human intestinal cell model of differentiated Caco-2 cells.

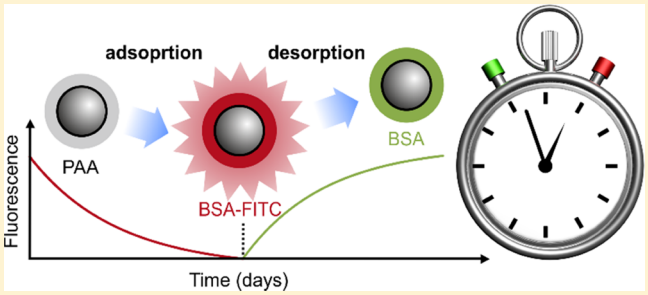

INTRODUCTION

During the last 5 years, there has been a rapid rise in the use of nanomaterials in consumer products. Especially, silver nanoparticles are frequently used because of their well-known optical and antimicrobial properties.[1] The products cover a wide range from toothpastes over children's toys to food containers.[2,3] From 2006, when ca. 25 products contained silver nanoparticles, the number of products today increased to 442 which corresponds to an 18-fold multiplication.[4,5] However, studies focusing on the toxicological potential of silver nanoparticles are highly controversial: there are investigations which claim an effect caused by the nanoscaled size of the particles, as well as studies which deny a "nanospecific effect".[6−8] As an example, De Matteis et al.[7] analyzed the interaction of silver nanoparticles with HeLa and A549 cells. They found that silver nanoparticles are degraded in the lysosomes and that the cell damage was predominantly caused by released silver ions, not by the nanoparticles. In contrast, Kim et al.[9] observed an increased cell death of MC3T3-E1 cells with decreasing size of silver nanoparticles, indicating a nanospecific effect. At the same time, both investigations suggest that the toxicology of silver nanoparticles strongly depends on their physicochemical properties and possible impurities. The main limitation is that often diverse types of nanoparticles, differing in size, surface coating, and dispersity, are used. The intensive characterization needed for specific toxicological assessment is often missing and is mostly connected with high costs and effort.

The use of reference materials provides the possibility to overcome this problem. They are thoroughly characterized particles with a narrow size distribution and are available for a variety of different nanomaterials.[10] Regarding biological investigations, a fluorescent marker is often used to monitor their transport and possible degradation.[11] For this purpose, the particles' ligand shell is either exchanged for a fluorescent stabilizer or the ligand is modified to include an emissive marker. A major challenge of fluorescence-labeled nanoparticles in biological application is: do we see the fluorescent marker which is attached to the particle or liberated fluorescent marker? Kreyling et al.[12] observed for gold nanoparticles which are coated by a thio-functionalized polymer—a ligand which is

Received: April 20, 2018
Revised: May 24, 2018
Published: May 24, 2018

DOI: 10.1021/acs.langmuir.8b01305
Langmuir 2018, 34, 7153−7160

known for a strong binding—a partial loss of the ligand in physiological environment.[13,14] Knowledge about the binding kinetics is important, because these markers are typically not covalently bound to the particles. Their adsorption and desorption onto the nanoparticles' surface is a dynamic process. Overall, relatively little is known about the binding behavior of fluorescent markers to nanoparticles and it is the aim of this study to contribute to this field.

Hence, we provide an investigation of the binding properties and kinetics of two different fluorescent ligands on small silver nanoparticles (Figure 1). Poly(acrylic acid) (PAA)-stabilized

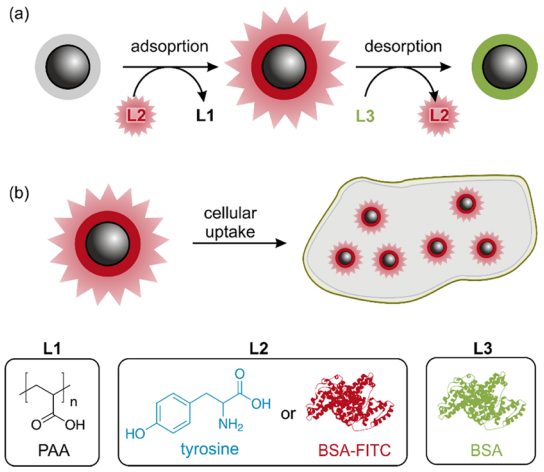

Figure 1. Scheme of adsorption and desorption experiments with the fluorescent labels tyrosine and BSA-FITC to silver nanoparticles.

small silver nanoparticles are available as a reference candidate material and were thoroughly characterized in a previous study.[15] The PAA ligand was exchanged for tyrosine or fluorescent-marked albumin (BSA-FITC). The adsorption of the ligands was monitored by dynamic light scattering (DLS). The fluorescent particles were characterized by small-angle X-ray scattering (SAXS), UV/vis, and fluorescence spectroscopy. Afterward, desorption of the ligands tyrosine and BSA-FITC was monitored by fluorescence spectroscopy, showing that the BSA-FITC/particle complex exhibits sufficient stability for laboratory applications. On the basis of these results, the BSA-FITC-labeled nanoparticles were used in first biological applications, namely cell viability tests, cellular uptake analyses, and in vitro imaging.

RESULTS AND DISCUSSION

Adsorption Process. The silver nanoparticles were synthesized according to an earlier reported procedure with slight modifications.[15] The particles are stabilized by PAA with an average molecular weight of 1800 g mol^{-1}. For the production of fluorescent-labeled particles, we have chosen two different molecules for ligand exchange: (i) tyrosine and (ii) BSA-FITC. Tyrosine is a non-essential amino acid and disposes a high biocompatibility. Because of the conjugation with the aromatic ring, the side chain is optically active. Typically, tyrosine is excited at wavelengths around 276 nm and emits at 310 nm. BSA-FITC is composed of the protein albumin and the fluorescent marker fluorescein isothiocyanate (FITC). BSA-FITC is excited between 480 and 500 nm and emits at 519 nm. As depicted in Figure 2, the two fluorescent labels were chosen because they show only a small overlap of

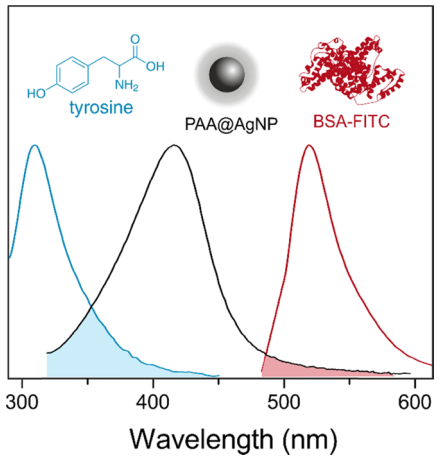

Figure 2. Normalized absorbance spectrum of PAA-stabilized silver nanoparticles (black line) and emission spectra of tyrosine (blue line) and BSA-FITC (red line) in water at 298 K. The areas where absorbance and emission spectra overlapped are marked by brighter colors.

their emission spectra with the absorbance band of the silver nanoparticles. Therefore, potential quenching effects caused by the spatial proximity to the silver nanoparticles are reduced. Nevertheless, a variety of conditions and molecular interactions, for example, molecular rearrangements, ground state complex formation, and collisional quenching, can result in fluorescence-quenching effects.[16]

The ligand exchange process was monitored by DLS. After addition of the new ligand, the hydrodynamic radius was changing with desorption of PAA and concurrent adsorption of tyrosine or BSA-FITC (Figure 3). The initial particles showed a hydrodynamic radius of R_h = 7.1 ± 0.4 nm (Figure 3b). We observed that for tyrosine the R_h decreased to 5.5 ± 0.3 nm immediately after addition of tyrosine. This radius did not change significantly over the time range of 196 h. In contrast, for the ligand exchange with BSA-FITC, the hydrodynamic radius increased slowly over time. Because BSA-FITC was added in excess (molar concentrations were 5.2 × 10^{-7} mol L^{-1} for BSA-FITC and 3.6 × 10^{-9} mol L^{-1} for silver nanoparticles), the reaction can be treated as a pseudo-first order reaction. Therefore, we used the following equation for data evaluation

$$R_h(t) = R_h(0) + \Delta R_h(1 - e^{-kt}) \quad (1)$$

In this equation, $R_h(0)$ is the initial hydrodynamic radius before ligand exchange, ΔR_h is the extrapolated increase of $R_h(0)$ for infinite times, k is a formal rate constant, and t is the experimental time in hours. The curve fit with its 95% confidence interval is shown in Figure 3a (R^2 value of the fit was 0.98). With the best fit value for ΔR_h of 3.6 ± 0.2 nm, we determined the value for the final hydrodynamic radius R_h = 10.7 ± 0.4 nm. This value is close to the experimental finding after 3 days and later. We calculated the time when half of the ligand on the surface of the particles is exchanged as $t_{1/2} = \ln(2) \times k^{-1}$. The value for $t_{1/2}$ amounts to 26 ± 3 h for BSA-FITC. Therefore, the reaction time for a full conversion can be expected to be around 3 days. These findings show that the rate-determining step of the ligand exchange is the adsorption of the new ligand and that the reaction is mainly independent on the desorption of PAA.

To verify that the observed effects on the hydrodynamic radius originate from the successful ligand exchange and not

DOI: 10.1021/acs.langmuir.8b01305
Langmuir 2018, 34, 7153−7160

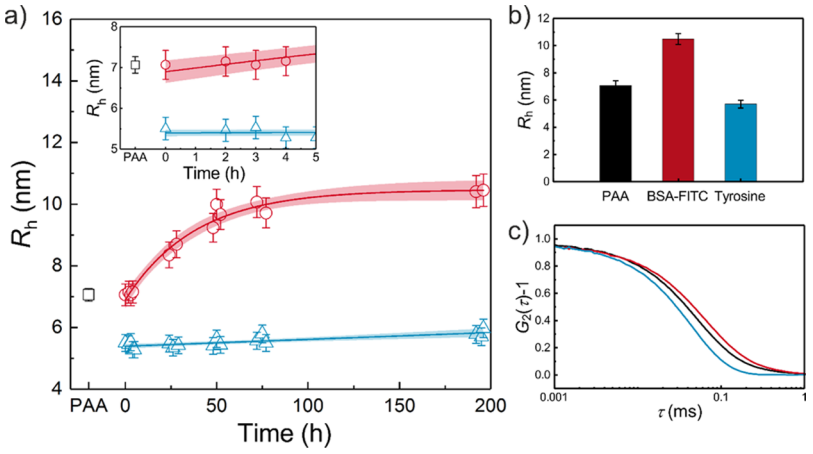

Figure 3. (a) DLS results for monitoring of the ligand exchange with BSA-FITC (red) and tyrosine (blue). Time-dependent hydrodynamic radius after addition of the new ligand is marked by symbols (red circles for BSA-FITC and blue triangles for tyrosine). The resulting fit for a first order reaction is given for BSA-FITC (solid red line), whereas for tyrosine a linear fit is displayed (solid blue line). Confidence bands at a 95% level are included (brighter areas). Inset: detailed view of the initial hydrodynamic radius and the first 5 h. (b) Final hydrodynamic radii before and after respective ligand exchange. (c) Correlation functions of the initial particles and the particles after ligand exchange.

from agglomeration or aggregation we used SAXS (Figure 4a). With SAXS, the size of the silver core can be determined

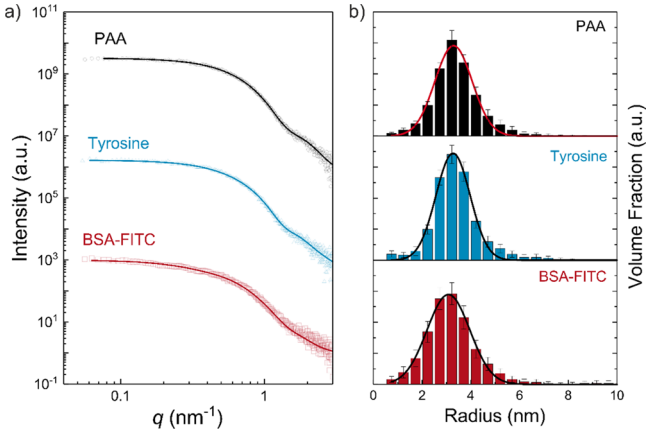

Figure 4. (a) SAXS data and corresponding curve fits (symbols and solid lines, respectively) of silver nanoparticles stabilized by PAA (black), tyrosine (blue), and BSA-FITC (red). The curves are shifted vertically for better visibility. (b) Volume-weighted size distributions (bars) derived from curve fits in (a). Gaussian fits of the size distributions are marked by solid lines (red for PAA, black for tyrosine and BSA-FITC).

because it scatters X-rays several orders of magnitude stronger than the surrounding shell of organic molecules. An advantage of SAXS is that a statistically relevant number of particles is recorded. From the SAXS curves, the volume-weighted size distribution of the particles was calculated with the help of a Monte Carlo-based evaluation method, which was proven suitable for precise size distribution quantification.[17,18] To determine the mean volume-weighted radius and the distribution width, the size distributions were approximated by a Gaussian function (Figure 4b). The mean volume-weighted radius of the initial particles was $R_{v,PAA}$ = 3.1 ± 0.1 nm, whereas the radii after ligand exchange with tyrosine and BSA-FITC amounted to $R_{v,tyrosine}$ = $R_{v,BSA-FITC}$ = 3.3 ± 0.1 nm. Thus, the size distribution of the particle cores did not change substantially upon ligand exchange.

The results of the SAXS evaluation are in agreement with the imaging data obtained via scanning transmission electron microscopy (STEM), as depicted in Figure 5. The particles were spherical and showed no sign of aggregation after successful ligand exchange.

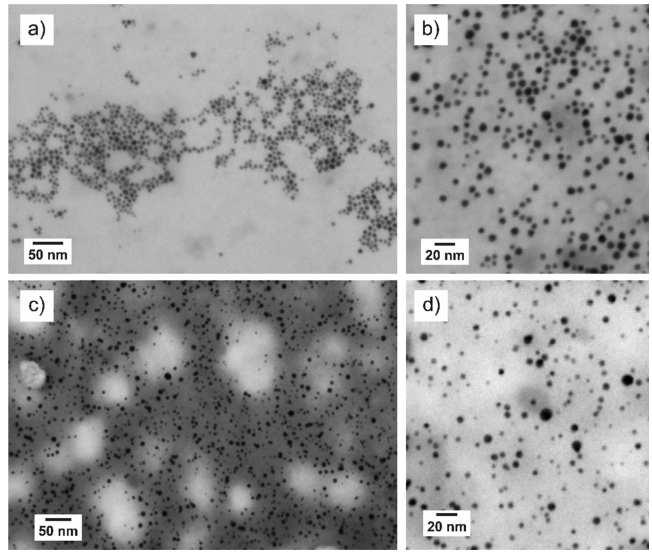

Figure 5. STEM images of the trans-functionalized silver nanoparticles at different magnifications: (a,b) show tyrosine-stabilized nanoparticles (scale bars are 50 and 20 nm); (c,d) show BSA-FITC-stabilized nanoparticles (scale bars are 50 and 20 nm) after successful ligand exchange.

The fluorescent properties of the trans-functionalized particles were characterized by fluorescence spectroscopy (Figure 6). From the comparison of the fluorescence emission spectra of the particles coated with tyrosine or BSA-FITC with their corresponding free analogs (without particles, same concentration), we assume that the silver nanoparticles induce fluorescence quenching. This is in accordance with the literature, where silver nanoparticles are described as a highly efficient quencher for fluorescence.[19] We found that the fluorescence intensity of the BSA-FITC-stabilized particles

DOI: 10.1021/acs.langmuir.8b01305
Langmuir 2018, 34, 7153−7160

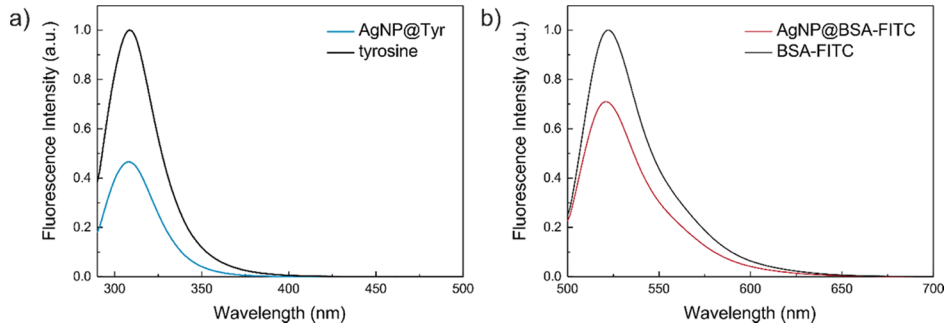

Figure 6. Fluorescence emission spectra of (a) tyrosine and (b) BSA-FITC (black curves) in comparison with the corresponding stabilized silver nanoparticles (blue and red curve, respectively). Excitation wavelengths were 276 nm for tyrosine and 487 nm for BSA-FITC.

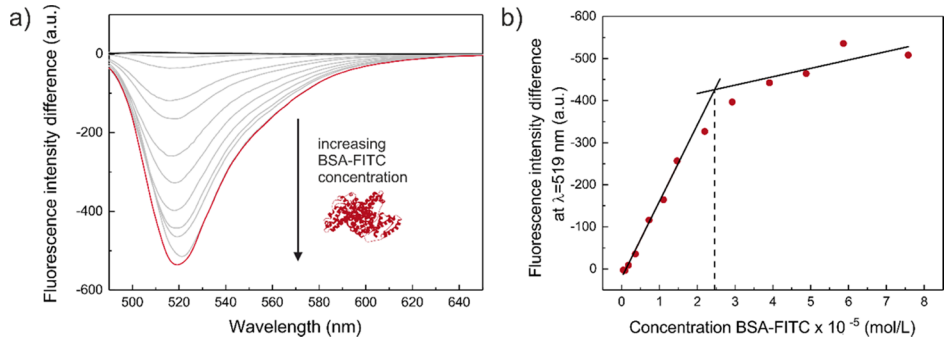

Figure 7. (a) Difference of fluorescence spectra of silver nanoparticles stabilized by BSA-FITC ($I_{BSA\text{-}FITC}$) and of the system without nanoparticles (I_{ref}): $I_{BSA\text{-}FITC} - I_{ref}$. Different BSA-FITC concentrations were used, ranging from 0.5 μM (black curve) to 75.8 μM (red curve). (b) Displayed are the intensities at 519 nm of (a) in dependence of the BSA-FITC concentration (red circles). Crossing of the two tangents (black lines) represents the equivalence point which gives the ratio of BSA-FITC molecules per silver nanoparticle of 20 ± 9.

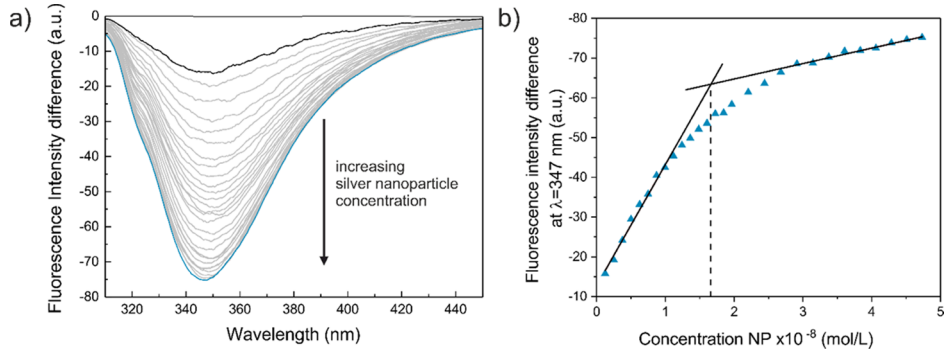

Figure 8. (a) Difference of fluorescence spectra of silver nanoparticles stabilized by tyrosine (I_{tyr}) and of the system without nanoparticles (I_{ref}): $I_{tyr} - I_{ref}$. Silver nanoparticles were titrated against a constant tyrosine solution silver nanoparticle concentrations ranging from 1.3 nM (black curve) to 47.3 nM (blue curve). (b) Displayed are the intensities at 347 nm of (a) in dependence of the silver nanoparticle concentration (blue triangles). Crossing of the two tangents (black lines) represents the equivalence point, which gives the ratio of tyrosine molecules per silver nanoparticle of 15 900 ± 200.

was 70% of the intensity of pure BSA-FITC at the fluorescence maximum of 520 nm. For the tyrosine-stabilized particles, we observed a stronger fluorescence quenching of 54% at the emission maximum of 310 nm. However, the remaining fluorescence intensity was intensive enough for the intended application of these particles in biological investigations.

A parameter of high interest is the amount of surface-bound ligands.[20−22] Especially, its quantitative determination in situ remains challenging. We used a fluorescence titration method to elucidate this issue. With this technique, the fluorescent ligand is titrated against the nanoparticles. The increase in the fluorescent signal allows the calculation of the amount of surface-bound ligand. For the adsorption of BSA-FITC, the changes in fluorescence quenching in comparison with the system without nanoparticles are displayed in Figure 7a. The fluorescence intensity reaches a limit where the fluorescence of further added ligand is not quenched (Figure 7b). Thus, the particle surface coverage by the fluorescent BSA-FITC ligand has reached saturation and additional ligands diffuse "freely" in solution. The point where the curve of Figure 7b reaches the saturation region corresponds to the intersection of two tangents, which approximate the linear curve progression in the beginning and at the end. We calculated that the silver nanoparticle surface is covered by 20 ± 9 BSA-FITC molecules.[23] This corresponds in approximation to a monolayer of the ligand (see Supporting Information).

DOI: 10.1021/acs.langmuir.8b01305
Langmuir 2018, 34, 7153−7160

For the tyrosine-stabilized particles, the silver nanoparticles were titrated against a known amount of tyrosine. By a similar data evaluation as previously described, the amount of surface-bound ligand was determined (Figure 8). For tyrosine, this corresponded to an amount of 15 900 ± 200 molecules per nanoparticle, which would imply a multilayered structure on the particle surface. At a first glance, the high number of tyrosine molecules is in contrast with the results of the DLS because the ligand shell should be larger than 2.2 nm (~0.6 nm would correspond to a tyrosine monolayer). A possible explanation for this discrepancy is the formation of a hard and soft corona of tyrosine similar to that reported for many proteins.[24−26] Because the nanoparticles were filtered before DLS measurements, the soft corona can be potentially sheared off during sample preparation. To verify this hypothesis, we again measured DLS of the tyrosine-stabilized nanoparticles without previous filtration. The measured hydrodynamic radius was substantially higher (R_h = 7.8 ± 0.5 nm, 4.5 nm shell thickness) and, thus, affirmed the assumption of a hard and a soft corona.

Desorption Process. Toxicological studies of nanoparticles often comprise in vitro and in vivo studies where the transport, uptake, and a possible accumulation of the particles can be observed. The use of a fluorescent maker is, therefore, a common concept to provide traceability. Important information which is often not taken into account is: how long does the fluorescent marker remain on the particle surface in physiological environment? We designed an experiment to give an approximation for this time span: the BSA-FITC-stabilized particles were diluted with a concentrated (20 g/L) solution of not fluorescent-labeled BSA. Fluorescence intensity was expected to increase when BSA-FITC of a population in the vicinity to the silver core is exchanged for BSA and released into the bulk solvent, because due to the exchange, fluorescence is not quenched anymore and increases as long as BSA-FITC is released. For our experiment, we have chosen two different dilutions (1:300 and 1:3000) of the silver nanoparticles to give an insight into desorption time spans (Figure 9). As a control experiment, the particles were diluted in phosphate-buffered saline (PBS), which is the matrix for BSA in the exchange experiment. Therein, the fluorescence intensity of the BSA-FITC-stabilized nanoparticles was normalized to 1 after a 1:300 dilution in PBS. The intensity of this mixture was in equilibrium instantaneously and remained constant for 12 days. In contrast, in the same time interval (12 days after mixing), the fluorescence intensity of the mixture of BSA-FITC-stabilized particles with BSA increased from 0.45 to ca. 0.6 for a dilution of 1:300 and from 0.45 to 1.0 for a dilution of 1:3000. Thus, it is obvious that a very high dilution and long incubation times are needed to remove BSA-FITC from the particles.

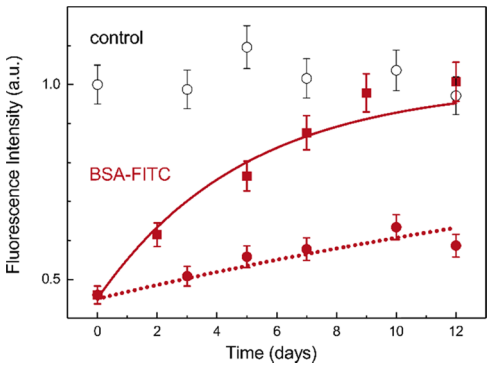

Figure 9. Fluorescence intensity at 519 nm as a function of time after mixing of BSA-FITC-stabilized silver nanoparticles with a solution of native BSA (not fluorescence-labeled) with a dilution of 1:300 (red circles) and 1:3000 (red squares), with respect to the nanoparticles. Curve fits of a pseudo first-order reaction reveal τ-values of 21 ± 3 days (1:300 dilution, dotted red line) and 3.4 ± 0.4 days (1:3000 dilution, solid red line). The results of the control experiment (mixing of BSA-FITC-stabilized silver nanoparticles with PBS) is marked by black circles.

For the quantification of the release of BSA-FITC, we applied a simple model. We utilized, corresponding to the adsorption process, a similarly modified first-order reaction kinetic rate equation $I_f(t) = I_f(0) + \Delta I_f(1 - e^{-kt})$. The $I_f(t)$ is the fluorescence intensity at time t, $I_f(0)$ is the fluorescence intensity at t = 0, and ΔI_f is the extrapolated value for the increase of the fluorescence intensity for infinite time, k is a formal rate constant, and t is the experimental time in hours. To avoid ambiguous results, we used constant values of $I_f(0)$ = 0.45, and ΔI_f = 0.55 to fulfill the normalization condition $I_f(0) + \Delta I_f = 1$ at infinite time. Therefore, only k remained as the free fit parameter. The k-values can be utilized to calculate the time τ required to release 50% of BSA-FITC contained in ΔI_f by $\tau = \ln(2) \times k^{-1}$. The resultant τ-value is 21 ± 3 days for a dilution of 1:300 and 3.4 ± 0.4 days for the 1:3000 dilution. Therefore, we assume that the release of BSA-FITC from the vicinity of the silver cores is in the order of days for the high 1:3000 dilution and in the order of weeks for the lower 1:300 dilution. This shows that the binding of BSA-FITC to the particles is relatively strong. We conclude that there is no indication for a substantial risk that the BSA-FITC-stabilized particles lose their fluorescent corona due to dilution when used, for example, in cell experiments for toxicological studies.

The same experiment was conducted with the tyrosine-stabilized nanoparticles, where no slow increase in the fluorescence intensity was observed after addition of BSA (see Supporting Information Figure S1). We conclude that similar to the fast adsorption of tyrosine, it is also quickly released which results in a constant fluorescence signal after addition. Therefore, we assume that it was not possible to monitor the exchange process because it was too fast and with the first UV/vis measurement directly after addition (t = 0) the desorption process was already completed. Furthermore, the stronger binding of the BSA by thiol groups outranges the adsorption of tyrosine via carbonyl groups and, therefore, supports the fast desorption. We conclude that the exchange of tyrosine is fully completed in the time range of seconds.

Biological Application. On the basis of the adsorption and desorption experiments, the BSA-FITC-stabilized silver nanoparticles were proven to be suitable for the investigation of their uptake and cellular localization in in vitro experiments. Therefore, we selected two cell models: (1) the liver cell model HepG2, which is a very commonly used hepatocyte in vitro model, and (2) the most common cell model for the intestinal enterocytes, differentiated Caco-2 cells. Both cell types were incubated with noncytotoxic concentrations of BSA-FITC marked silver nanoparticles up to 24 h (for cell viability data, see Supporting Information Figure S2). Representative confocal images are given in Figure 10. They show a time-dependent uptake of silver nanoparticles in HepG2 cells with some nanoparticles having cell contact after 2 h, and numerous particles deep inside the cells after 24 h. In contrast to that, the differentiated Caco-2 monolayer showed just a few particles in

DOI: 10.1021/acs.langmuir.8b01305
Langmuir 2018, 34, 7153−7160

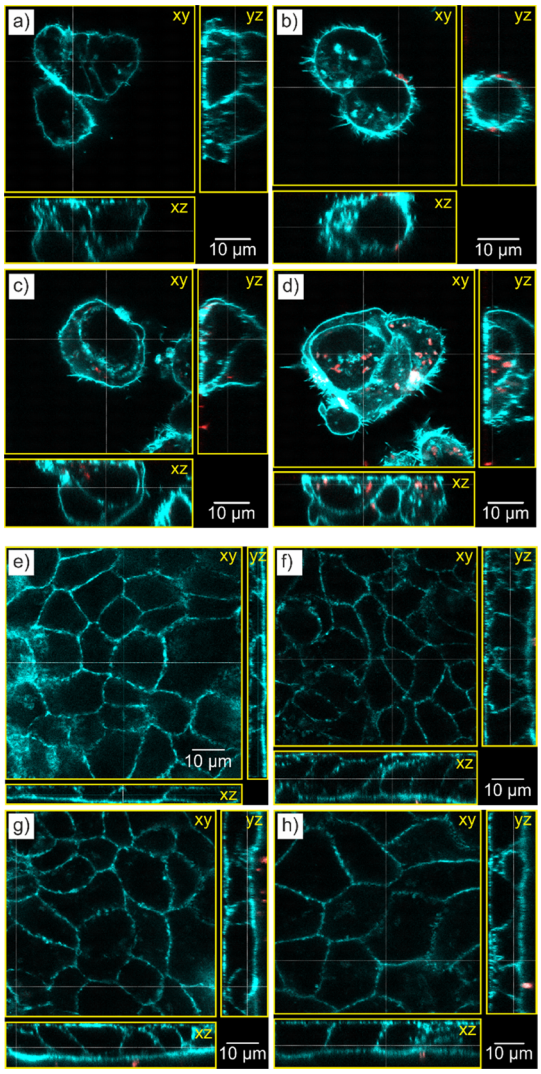

Figure 10. Confocal fluorescence microscopy images of HepG2 (a–d) and differentiated Caco-2 cells (e–h). The cell lines were incubated with BSA-FITC-stabilized particles for 2, 6, and 24 h (b–d for HepG2 and f–h for Caco-2 cells). A control sample for each cell line shows the status without silver nanoparticles (a,e). From preliminary cytotoxicity tests, noncytotoxic silver concentrations of 10 and 25 μg/mL were chosen for HepG2 and Caco-2 cells, respectively. The images show the view in *xy*, *xz*, and *yz* direction (yellow boxes), whereas the dotted white lines mark the plane, from which the other cutting planes are derived. The cytoskeleton is stained by ActinRed 555 marked with blue color, whereas the BSA-FITC-stabilized particles are marked by red color.

contact with the microvilli brush border on the apical side of the monolayer for all time points and almost no particles inside the cells. Therefore, the fluorescence labeling-enabled time-dependent uptake studies showed clear differences in particle uptake for cells from different tissues.

CONCLUSIONS

The process of fluorescent ligand adsorption and desorption on silver nanoparticles has been monitored by DLS, SAXS, and fluorescence spectroscopy. The fluorescent ligands BSA-FITC and tyrosine were compared. According to DLS, tyrosine shows substantially faster adsorption kinetics, whereas the ligand exchange with BSA-FITC takes at least 3 days. For BSA-FITC, the amount of stabilizer corresponds to a monolayer, whereas tyrosine shows the formation of a multilayered hard and soft corona. In a desorption experiment, it was shown that BSA-FITC exhibits a long residence time in the range of days, in contrast to tyrosine which desorbs as fast as it adsorbs. Therefore, the BSA-FITC-stabilized particles are suitable for application in biological studies. As an example, we provided data from human HepG2 and Caco-2 cells. The latter show no substantial uptake, whereas cellular uptake was found for HepG2 cells already after 2 h. The present study on persistently fluorescence-labeled silver nanoparticles opens the pathway for further comparable biological investigations regarding uptake, excretion, or toxicity. Our standardized and thoroughly characterized reference candidate material is well-suited for this purpose.

MATERIALS AND METHODS

Materials. All chemicals were used as received without further purification. PAA (M_w = 1800 g/mol), BSA, BSA-FITC, and PBS were purchased from Sigma-Aldrich; NaOH, ethylene glycol, and (*S*)-(−)-tyrosine from Merck and silver nitrate from AppliChem. Ultrapure water was used for all preparations (Milli-Q, 18.2 mΩ at 25 °C).

Synthesis of Silver Nanoparticles. The synthesis of PAA stabilized particles was performed according to a previous description.[27] We repeated the synthesis several times to ensure reproducibility. It will be briefly described: first, a solution of 1.9 g (11.4 mmol) of silver nitrate in 58.5 mL of ethylene glycol was prepared at room temperature. In a 500 mL-three-necked flask, 15.7 g (217.9 mmol with respect to the monomer units) of PAA with an average molecular weight of M_w = 1800 g/mol was added to 291.5 mL of ethylene glycol and heated under stirring to 200 °C. Afterward, the silver nitrate solution was added within 3 s to the boiling solution under stirring. The mixture was refluxed for 15 min and then cooled to room temperature. For purification of the particles, 800 mL of water (pH = 5) was added and the mixture was stored for 24 h. Thereafter, the reddish brown supernatant was decanted. This washing procedure was repeated three times. The resulting residue was suspended in 150 mL of water, and a 1% (w/v) sodium hydroxide solution was added dropwise until the pH of the dispersion was adjusted to a value of 10. During this procedure, the color of the dispersion turned from reddish brown, via olive-green to brownish black. Finally, PAA (0.2 mmol in water) was added to provide a better long term colloidal stability. The concentration of elementary silver was determined by SAXS and amounts to 2.9 g/L.

Ligand Exchange with BSA-FITC and Tyrosine. For the ligand exchange with BSA-FITC, 1 mL of the initial particle dispersion was placed in a glass vial, and a mixture of 0.5 mL BSA-FITC (0.15 μmol), and 1 mL NaOH (0.1 M) was added. The mixture was stirred for 3 days.

For the ligand exchange with tyrosine, 2.5 mL of the initial particle dispersion was placed in a vial, and 1.2 mL of tyrosine (24.3 mg, 0.13 mmol) in NaOH solution (1 wt %) was added under stirring.

DLS Measurements. The DLS measurements were performed using a multi-angle ALV Instrument (ALV 7004, ALV Langen) equipped with a He–Ne laser (λ = 632.8 nm). Data were recorded at 23 ± 1 °C at scattering angles of 2θ = 26°–146° (8°-steps). Six measurement cycles were conducted with 60 s for each angle. For measurement, the samples were diluted 1:100 with water or NaOH solution (0.1 M). Curve fitting was conducted with the software MCDLS (version 1.0.1).

SAXS Measurements. SAXS measurements were performed in a flow through capillary with a Kratky-type instrument (SAXSess from Anton Paar, Austria) at 21 ± 1 °C. Samples analyzed with SAXS were used as prepared and measured for 20 min (120 measurement frames averaged over 10 s). The measured scattering data were corrected by subtracting the data of a capillary filled with pure water. The measured intensity was converted to absolute scale according to Orthaber et al.[28] The scattering vector q depends on the wavelength λ of the radiation

DOI: 10.1021/acs.langmuir.8b01305
Langmuir 2018, 34, 7153–7160

(λ = 0.154 nm), and thus, $q = 4\pi/\lambda \sin\theta$. Deconvolution (slit length desmearing) of the SAXS curves was performed with the SAXS-Quant software (Anton Paar, Austria). Curve fitting was conducted with the software McSAS[18] (version 1.3).

STEM-Imaging. The STEM images were obtained from a Zeiss Gemini SUPRA 40 scanning electron microscope operating at transmission mode at 10−20 kV. The TEM grids were prepared by placing 2 μL of the particle dispersion on a carbon grid and drying at room temperature.

Fluorescence Spectroscopy. The fluorescence measurements were performed using a Fluorolog spectrofluorometer from HORIBA and a spectrofluorometer FB-6500 from JASCO. The emission spectra of tyrosine and tyrosine-stabilized particles were recorded using an excitation wavelength of 276 nm. The emission spectra of BSA-FITC and BSA-FITC-stabilized nanoparticles were recorded using an excitation wavelength of 487 nm. The dispersions were diluted with water (tyrosine) or PBS (BSA-FITC) in a ratio of 1:100. Experimental details of the titration and desorption experiments are described in the Supporting Information.

Cell Culture Experiments. The human colon adenocarcinoma cell line Caco-2 and the human liver hepatocellular carcinoma cell line HepG2 were obtained from the European Collection of Cell Cultures (ECACC, Porton Down, UK). Cells were maintained in Dulbecco's modified Eagle's medium, supplemented with 10% fetal calf serum and 1% penicillin and streptomycin at 37 °C in a humidified atmosphere of 5% CO_2. Cells were maintained in tissue culture flasks (75 cm^2) as a subconfluent monolayer for propagation. For microscopically analysis of particle uptake, 55 000 cells were seeded per 12 well on cover slides. HepG2 cells were grown over night and Caco-2 cells were differentiated for 21 days (medium was changed every 2 to 3 days). Cells were incubated with noncytotoxic concentrations of fluorescence marked silver nanoparticles (for cell viability analysis, see Supporting Information). After 2, 6, and 24 h, cells were washed twice with PBS, fixated for 10 min with 3.7% formaldehyde, washed three times with PBS with Tween, permeabilized with 0.2% Triton X-100 for 10 min, washed again three times with PBS, stained with ActinRed 555 Ready Probes Reagent (Invitrogen), and washed one last time. Samples were analyzed by SP5 confocal fluorescence microscopy from Leica Microsystems.

■ ASSOCIATED CONTENT

Supporting Information

The Supporting Information is available free of charge on the ACS Publications website at DOI: 10.1021/acs.langmuir.8b01305.

Experimental details; desorption of tyrosine; and cell viability data (PDF)

■ AUTHOR INFORMATION

Corresponding Author

*E-mail: andreas.thuenemann@bam.de. Phone: +49 3081041610.

ORCID

Claudia Kästner: 0000-0003-3730-7404

Linda Böhmert: 0000-0002-1153-2841

Andreas F. Thünemann: 0000-0002-9883-6134

Notes

The authors declare no competing financial interest.

■ ACKNOWLEDGMENTS

We gratefully thank S. Benemann and D. Hodoroaba for the STEM measurements of the nanoparticles. Additionally, we also thank the group of C. A. Schalley and R. Haag for the possibility to use their spectrofluorometers. A great thanks goes also to H. V. Schröder for productive discussion of the manuscript.

■ REFERENCES

(1) Nowack, B.; Krug, H. F.; Height, M. 120 Years of Nanosilver History: Implications for Policy Makers. *Environ. Sci. Technol.* **2011**, *45*, 1177−1183.

(2) Duncan, T. V. Applications of nanotechnology in food packaging and food safety: Barrier materials, antimicrobials and sensors. *J. Colloid Interface Sci.* **2011**, *363*, 1−24.

(3) Wijnhoven, S. W. P.; Peijnenburg, W. J. G. M.; Herberts, C. A.; Hagens, W. I.; Oomen, A. G.; Heugens, E. H. W.; Roszek, B.; Bisschops, J.; Gosens, I.; Van De Meent, D.; Dekkers, S.; De Jong, W. H.; van Zijverden, M.; Sips, A. J. A. M.; Geertsma, R. E. Nano-silver − a review of available data and knowledge gaps in human and environmental risk assessment. *Nanotoxicology* **2009**, *3*, 109−138.

(4) Vance, M. E.; Kuiken, T.; Vejerano, E. P.; McGinnis, S. P.; Hochella, M. F., Jr.; Rejeski, D.; Hull, M. S. Nanotechnology in the real world: Redeveloping the nanomaterial consumer products inventory. *Beilstein J. Nanotechnol.* **2015**, *6*, 1769−1780.

(5) Mehboob, S.; Jacob, J.; May, M.; Kotula, L.; Thiyagarajan, P.; Johnson, M. E.; Fung, L.W.-M. Structural analysis of the alpha N-terminal region of erythroid and nonerythroid spectrins by small-angle X-ray scattering. *Biochemistry* **2003**, *42*, 14702−14710.

(6) Xiu, Z.-M.; Zhang, Q.-B.; Puppala, H. L.; Colvin, V. L.; Alvarez, P. J. J. Negligible Particle-Specific Antibacterial Activity of Silver Nanoparticles. *Nano Lett.* **2012**, *12*, 4271−4275.

(7) De Matteis, V.; Malvindi, M. A.; Galeone, A.; Brunetti, V.; De Luca, E.; Kote, S.; Kshirsagar, P.; Sabella, S.; Bardi, G.; Pompa, P. P. Negligible particle-specific toxicity mechanism of silver nanoparticles: The role of Ag+ ion release in the cytosol. *Nanomedicine* **2015**, *11*, 731−739.

(8) Haase, A.; Rott, S.; Mantion, A.; Graf, P.; Plendl, J.; Thünemann, A. F.; Meier, W. P.; Taubert, A.; Luch, A.; Reiser, G. Effects of Silver Nanoparticles on Primary Mixed Neural Cell Cultures: Uptake, Oxidative Stress and Acute Calcium Responses. *Toxicol. Sci.* **2012**, *126*, 457−468.

(9) Kim, T.-H.; Kim, M.; Park, H.-S.; Shin, U. S.; Gong, M.-S.; Kim, H.-W. Size-dependent cellular toxicity of silver nanoparticles. *J. Biomed. Mater. Res., Part A* **2012**, *100*, 1033−1043.

(10) Stefaniak, A. B.; Hackley, V. A.; Roebben, G.; Ehara, K.; Hankin, S.; Postek, M. T.; Lynch, I.; Fu, W.-E.; Linsinger, T. P. J.; Thünemann, A. F. Nanoscale reference materials for environmental, health and safety measurements: needs, gaps and opportunities. *Nanotoxicology* **2013**, *7*, 1325−1337.

(11) Henrich-Noack, P.; Prilloff, S.; Voigt, N.; Jin, J.; Hintz, W.; Tomas, J.; Sabel, B. A. In vivo visualisation of nanoparticle entry into central nervous system tissue. *Arch. Toxicol.* **2012**, *86*, 1099−1105.

(12) Kreyling, W. G.; Abdelmonem, A. M.; Ali, Z.; Alves, F.; Geiser, M.; Haberl, N.; Hartmann, R.; Hirn, S.; de Aberasturi, D. J.; Kantner, K.; Khadem-Saba, G.; Montenegro, J.-M.; Rejman, J.; Rojo, T.; de Larramendi, I. R.; Ufartes, R.; Wenk, A.; Parak, W. J. In vivo integrity of polymer-coated gold nanoparticles. *Nat. Nanotechnol.* **2015**, *10*, 619−623.

(13) Chen, H.; Zou, P.; Connarn, J.; Paholak, H.; Sun, D. Intracellular dissociation of a polymer coating from nanoparticles. *Nano Res.* **2012**, *5*, 815−825.

(14) Henriksen-Lacey, M.; Carregal-Romero, S.; Liz-Marzán, L. M. Current Challenges toward In Vitro Cellular Validation of Inorganic Nanoparticles. *Bioconjugate Chem.* **2017**, *28*, 212−221.

(15) Kästner, C.; Thünemann, A. F. Catalytic Reduction of 4-Nitrophenol Using Silver Nanoparticles with Adjustable Activity. *Langmuir* **2016**, *32*, 7383−7391.

(16) Saha, K.; Agasti, S. S.; Kim, C.; Li, X.; Rotello, V. M. Gold Nanoparticles in Chemical and Biological Sensing. *Chem. Rev.* **2012**, *112*, 2739−2779.

(17) Pauw, B. R.; Kästner, C.; Thünemann, A. F. Nanoparticle size distribution quantification: results of a small-angle X-ray scattering inter-laboratory comparison. *J. Appl. Crystallogr.* **2017**, *50*, 1280−1288.

DOI: 10.1021/acs.langmuir.8b01305
Langmuir 2018, 34, 7153−7160

(18) Bressler, I.; Pauw, B. R.; Thünemann, A. F. McSAS: software for the retrieval of model parameter distributions from scattering patterns. *J. Appl. Crystallogr.* **2015**, *48*, 962−969.
(19) Ghosh, D.; Chattopadhyay, N. Gold and silver nanoparticles based superquenching of fluorescence: A review. *J. Lumin.* **2015**, *160*, 223−232.
(20) Schindler, T.; Schmiele, M.; Schmutzler, T.; Kassar, T.; Segets, D.; Peukert, W.; Radulescu, A.; Kriele, A.; Gilles, R.; Unruh, T. A Combined SAXS/SANS Study for the in Situ Characterization of Ligand Shells on Small Nanoparticles: The Case of ZnO. *Langmuir* **2015**, *31*, 10130−10136.
(21) Liu, X.; Guan, Y.; Ma, Z.; Liu, H. Surface modification and characterization of magnetic polymer nanospheres prepared by miniemulsion polymerization. *Langmuir* **2004**, *20*, 10278−10282.
(22) Gupta, A. K.; Gupta, M. Synthesis and surface engineering of iron oxide nanoparticles for biomedical applications. *Biomaterials* **2005**, *26*, 3995−4021.
(23) Thordarson, P. Determining association constants from titration experiments in supramolecular chemistry. *Chem. Soc. Rev.* **2011**, *40*, 1305−1323.
(24) Walkey, C. D.; Chan, W. C. W. Understanding and controlling the interaction of nanomaterials with proteins in a physiological environment. *Chem. Soc. Rev.* **2012**, *41*, 2780−2799.
(25) Micl̆auş, T.; Bochenkov, V. E.; Ogaki, R.; Howard, K. A.; Sutherland, D. S. Spatial Mapping and Quantification of Soft and Hard Protein Coronas at Silver Nanocubes. *Nano Lett.* **2014**, *14*, 2086−2093.
(26) Milani, S.; Baldelli Bombelli, F.; Pitek, A. S.; Dawson, K. A.; Rädler, J. Reversible versus Irreversible Binding of Transferrin to Polystyrene Nanoparticles: Soft and Hard Corona. *ACS Nano* **2012**, *6*, 2532−2541.
(27) Kästner, C.; Thünemann, A. F. Catalytic Reduction of 4-Nitrophenol Using Silver Nanoparticles with Adjustable Activity. *Langmuir* **2016**, *32*, 7383−7391.
(28) Orthaber, D.; Bergmann, A.; Glatter, O. SAXS experiments on absolute scale with Kratky systems using water as a secondary standard. *J. Appl. Crystallogr.* **2000**, *33*, 218−225.

DOI: 10.1021/acs.langmuir.8b01305
Langmuir 2018, 34, 7153−7160